Hindawi
Advances in Materials Science and Engineering
Volume 2018, Article ID 4059675, 15 pages
https://doi.org/10.1155/2018/4059675

Research Article

Behavior of Concrete-Filled Steel Tube Columns Subjected to Axial Compression

Pengfei Li, Tao Zhang, and Chengzhi Wang

Chongqing Jiaotong University, Chongqing 400074, China

Correspondence should be addressed to Pengfei Li; lipengfei@cqjtu.edu.cn

Received 21 March 2018; Revised 27 July 2018; Accepted 5 August 2018; Published 26 August 2018

Academic Editor: José A. Correia

The behavior of concrete-filled steel tube (CFST) columns subjected to axial compression was experimentally investigated in this paper. Two kinds of columns, including CFST columns with foundation and columns without foundation, were tested. Columns of pure concrete and concrete with reinforcing bars as well as two steel tube thicknesses were considered. The experimental results showed that the CFST column with reinforcing bars has a higher bearing capacity, more effective plastic behavior, and greater toughness, and the elastoplastic boundary point occurs when the load is approximately 0.4–0.5 times of the ultimate bearing capacity. The change of rock-socketed depth and the presence of steel tube will affect the ultimate bearing capacity of rock-socketed pile. The bearing capacities of the rock-socketed CFST columns are lower than those of rock-socketed columns without a steel tube under a vertical load; besides, the greater the rock-socketed depth, the greater the bearing capacity of the rock-socketed piles. In addition, a numerical comparison between the ultimate load and the theoretical value calculated from the relevant specifications shows that the ultimate load is generally considerably greater than the theoretical calculation results.

1. Introduction

In the last few decades, high-rise, large-span, and large-scale building structures have become more common. Concrete-filled steel tubular (CFST) members are well recognized for their excellent performance owing to the combined merits of steel and concrete materials [1]. Therefore, concrete-filled steel tubes are being increasingly used in high-rise buildings and in large-span structures. CFST columns have been used in earthquake-resistant structures and bridge piers subject to impact from traffic and used to support storage tanks, decks of railways, and high-rise buildings as well as being used as piles. Concrete-filled steel tubes require additional fire-resistant insulation if the fire protection of the structure is necessary [2].

Studies of CFST have also been frequently performed, and tests of CFST with rectangular, square, and circular cross sections filled with high-strength concrete have been reported [3–6], including compression [7–12], bending [13–17], or torsion [18–20] tests. The influence of the behavior and strength capacity of CFST on the bonding and local buckling of the steel profile, confinement of the concrete, and strength of the materials were discussed. Pull-out tests on CFST columns have shown the contribution of shear connectors to the force transference mechanism that occurs in beam-column connections. Local buckling has been widely studied, and it is possible to consider its influence on the strength capacity of the CFST columns. The confinement effect is influenced by the shape of the cross section, the thickness of the steel profile, the type of loading, the slenderness of the composite column, and the strength of the materials used. The studies on CFST rock-socketed columns and predicting the ultimate capacity of CFST columns subjected to axial compression are limited, and there is no standard method for calculating the strength of concrete-filled steel tube with reinforcing bars.

There are several design codes for concrete-filled steel columns, such as the America Institute of Steel Construction (AISC) Load and Resistance Factor Design (LRFD) [21], Eurocode 4 (EC4) [22], Brazilian Code NBR 8800 [23, 24], and GB50396-2014 [25]. Since the AISC is focused on steel columns, use of the AISC [21] specifications is limited to

composite columns with steel yield stress and concrete cylinder strength no greater than 415 and 55 MPa, respectively. Modified values for both the yielding strength (f_{my}) and elasticity modulus (E_m) are assumed. These modified terms take into account the presence of the concrete filling the steel profile. EC4 [22] and NBR 8800 [23, 24] determine the resistance capacity of a section by adding the contribution of the steel tube and the concrete core. For columns with circular cross sections, the confinement effect is considered by using coefficients that increase the uniaxial compressive strength of the concrete (f_{ck}) and reduce the yielding strength of the steel (f_y). The instability in these standard codes is considered by using a coefficient, which depends on the slenderness of the composite column. Limits for the steel tube slenderness are also considered to avoid local buckling.

In China, reinforced CFST piles are widely used in foundations of piers and bridges for its good mechanical properties, for instance, Orchard Container pier in Chongqing Port, Cuntan pier, Xintian Container pier in Wanzhou Port, and Yangshuo pier in Wuhan Port. The remarkable feature of this new structure is that the thickness of the steel pipe is thin and the ratio of diameter to thickness is very large [26]. It greatly exceeds the allowable range of the much existing specifications [27], for example, the ferrule coefficient of circular-section concrete-filled steel tubular members specified in Chinese specification [28] should be limited to between 0.3 and 3.0, and the ratio of diameter to thickness (D/t) should be limited to the following range: $20\sqrt{235/f_y} \le D/t \le 85\sqrt{235/f_y}$; Eurocode 4 (EC4) [22] explicit limits the allowed D/t values in the European context to $90 * 235/f_y$. The maximum allowable value of diameter-thickness ratio (D/t) specified in AISC [21] is $0.31 * E/f_y$. So, it is an attempt to estimate the ultimate load of reinforced CFST piles by above codes, and it may provide a reference for the design and research of the new structure with large diameter-to-thickness ratio.

The present paper is thus an attempt to study the behavior of concrete-filled steel tube columns with foundation and columns without foundation subjected to axial compression. The main objectives of this paper were twofold: first, to discuss the bearing capacity of CFST columns under vertical load with regard to the thickness of steel tube, reinforcement, and the depth of rock-socketing; second, to discuss the ultimate load experimental results and theoretical calculations.

2. Experimental Study

2.1. Columns without Foundation

2.1.1. Test Program. The experimental study of concrete-filled steel tube columns subjected to axial compression was accomplished with several objectives, namely, the evaluation of the accuracy of several design codes to predict the resistance capacity, to determine the maximum load capacity of the concentric loading specimens, and to investigate the failure pattern before and after the ultimate load is reached.

The specimens were tested; a summary of their properties is presented in Table 1, and the schematic of pile is shown in Figure 1. The cross sections of the tested columns are circular, the length of each column specimen is 1200 mm, and the diameters of the specimens are either 150 mm (symbolized with "1") or 165 mm (symbolized with "2"), thickness of the steel tube are either 1.2 mm (symbolized with "A") or 1.6 mm (symbolized with "B").

2.1.2. Properties of the Materials. The concrete was produced in the laboratory of the Structural Engineering Department, and the mechanical properties of the concrete core were determined by cylinder tests (150 mm × 150 mm × 150 mm). In addition, the concrete mix ratio is shown in Table 2. The concrete grade is C30, the mixing ratio of cement: sand: stone: water for ordinary Portland cement with a cement strength grade of M32.5 is 1 : 2.28 : 4.07 : 0.65 (mass ratio); the gravel underwent natural drying after washing, and it ranged from 5 to 10 mm in diameter. During the casting of the specimen, three standard concrete cube specimens of 150 mm × 150 mm × 150 mm are reserved for each batch of concrete, and the standard cube test block is sprinkled for 28 days for concrete axial compressive strength test. The compressive strength of concrete cube specimens is shown in Table 3. According to the yield strength test of steel bars, the stress-strain curve of steel bars is obtained. The yield strength of steel bars is 375 MPa, and the ultimate yield tensile strength is 410 MPa, as is shown in Table 3.

In Table 4, E is equal to the modulus of elasticity. A HRB335 steel plate is used for the steel-retaining material, and it is welded to a steel sleeve with a thickness of either 1.2 mm or 1.6 mm, and the steel bar is a two-stage rib bar with a diameter of 6 mm.

2.1.3. Test Setup. All of the tests were performed in a vertical column-testing machine with a static load capacity of 5000 kN, as is shown in Figure 2. The upper and lower surfaces of the column are, respectively, connected with the loading device and the rigid base plate by using a rigid pad. The load is divided into 12 stages according to the estimated ultimate carrying capacity, but the load grading is not consistent: during the initial stage, the loading is larger, but the loading grading is gradually reduced after the plastic stage of deformation is reached. This loading scheme allows the study of the post-peak behavior of the composite columns. Therefore, it is possible to study the elastic behavior, the axial load capacity, and the ductility of the columns under axial loading.

For this test, three layers of strain gauges were arranged vertically along the column, and the data were collected by a signal acquisition system to explore the variation in the strain of the steel casing with an applied load. Besides, the distance between the first strain gauge and the column top and the distance between the bottom strain gauge and the pile bottom were both 30 cm, and the distance between adjacent strain gauge layers was 30 cm. The 4 strain gauges in each layer were arranged symmetrically along the column surface. And an additional strain gauge was embedded in the

Table 1: List of columns for CFST columns without foundation.

Specimens	$D \times \delta \times L$ (mm)	Ac (mm^2)	Ar (mm^2)	As (mm^2)	α_{sc} (%)
PL-2	$165 \times 0 \times 1200$	21382	0	0	0
NS-A-2	$165 \times 1.2 \times 1200$	21382	0	622	2.9
NS-B-2	$165 \times 1.6 \times 1200$	21382	0	829	3.9
RN-2	$165 \times 0 \times 1200$	21382	170	0	0.8
RS-A-2	$165 \times 1.2 \times 1200$	21382	170	622	3.7
RS-B-2	$165 \times 1.6 \times 1200$	21382	170	829	4.7
PL-1	$150 \times 0 \times 1200$	17671	0	0	0
NS-A-1	$150 \times 1.2 \times 1200$	17671	0	570	3.2
RS-A-1	$150 \times 1.2 \times 1200$	17671	170	570	4.1
RS-B-1	$150 \times 1.6 \times 1200$	17671	170	762	5.2

Notation: D: outside diameter of the circular steel tube; δ: wall thickness of the steel tube; L: length of the specimens; Ac: concrete cross-sectional area; Ar: reinforced cross-sectional area; As: steel cross-sectional area; α_{sc}: steel ratio; PL: plain concrete; RS: concrete-filled steel tube column with reinforcing bars; NS: concrete-filled steel tube column without reinforcing bars; and RN: concrete column with reinforcing bars. A: thickness of steel tube is 1.2 mm; B: thickness of steel tube is 1.6 mm; 1: diameter is 150 mm; 2: diameter is 165 mm.

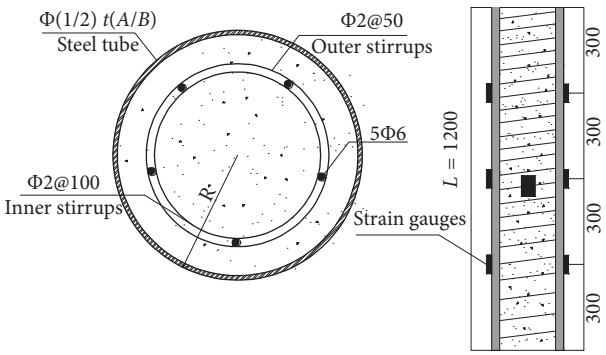

Figure 1: Schematic of the specimens and arrangement of the strain gauges around the columns.

Table 2: Concrete mix ratio.

Grade	Concrete mix ratio	Cement (kg/m^3)	Water (kg/m^3)	Stone (kg/m^3)	Sand (kg/m)
C30	0.65	300	195	1220	685

concrete, and the strain of the concrete was measured with the change in the load. In these tests, each strain gauge was divided into vertical and horizontal measuring points; therefore, 12 strain gauges, a total of 24 points, were placed on the outside of each specimen. Additionally, four displacement gauges are arranged symmetrically on the pile top and the pile bottom to measure the change in the compression of the pile with the load during the loading process; these results were used as the basis of the loading control method.

2.2. Columns with Foundation

2.2.1. Test Program. The test program for the columns with foundation is approximately consistent with that of the concrete-filled steel tube columns without foundation; the cross sections of these columns are also circular, and all the columns were filled with C30 concrete. The specimens were tested, and a summary of their properties is presented in Table 5. The length of each column specimen is 800 mm, the diameter of each is 100 mm, and the size of foundation is 2.1 m × 1.3 m × 1 m.

Table 3: Mechanical properties of the concrete and steel tube.

Specimens	f_{cu} (MPa)	f_y (MPa)
PL-2	32.1	—
NS-A-2	34.6	375
NS-B-2	34.9	375
RN-2	31.2	375
RS-A-2	33.7	375
RS-B-2	33.5	375
PL-1	34.8	—
NS-A-1	32.9	375
RS-A-1	33.4	375
RS-B-1	34.1	375

Table 4: Material properties of the concrete and steel tube.

Types	Grade	E (MPa)	N
Concrete	C30	$2.75E+04$	0.2
Reinforcement	HRB335	$2.10E+05$	0.3
Steel	HRB335	$2.10E+05$	0.3
Stirrups	HRB335	$2.10E+05$	0.3

2.2.2. Properties of the Materials. The concrete for the columns was produced with high-strength M30 cement mortar, with a cement: quartz: sand: water mix ratio of 1 : 1.76 : 0.32 (mass ratio). The diameter of the steel tube is 100 mm, its thickness is 1 mm, and its elastic modulus is approximately $E = 200$ GPa. Additionally, the main bar of secondary reinforcement has a diameter of 6 mm, and the stirrups have a diameter of 1 mm. The stirrups spacing is 3 cm in the column.

Due to the large size of the test foundations, they cannot be excavated to the laboratory, so concrete was used to simulate the rock foundation. Mudstone is susceptible to weathering, which leads to a reduction in the bearing capacity of the pile; therefore, the concrete strength is low to simulate strong weathering mudstones. The concrete mix ratio is 12.5% cementitious material, 12.5% stone, and 50% sand. After 28 days of curing, testing results showed that the compressive strength of the standard concrete was 300 KPa, and the elastic modulus was 16 MPa.

The pile was formed as shown in Figure 3. In addition, the material properties of the concrete core and steel tube are shown in Table 6.

2.2.3. Test Setup. The loading system uses a split hydraulic jack with a limit load of 200 kN. When the loading device is installed, the load sensor can be placed on a piece of steel plate on top of the pile, and the loading apparatus is a separate hydraulic jack that is placed on top. The top of the

(a) (b)

Figure 2: Test setup. (a) General view. (b) CFST detail.

Table 5: List of columns for CFST columns with foundation.

Specimens	D (mm)	h (mm)	n ($n = h/D$)	Steel tube (mm)
Z1P1	100	300	3	1
Z1P2	100	300	3	0
Z2P1	100	400	4	1
Z2P2	100	400	4	0
Z3P1	100	500	5	1
Z3P2	100	500	5	0

Notation: Z1: rock-socketed depth is 300 mm; Z2: rock-socketed depth is 400 mm; Z3: rock-socketed depth is 500 mm; P1: steel tube is 1 mm; P2: steel tube is 0 mm; h: rock-socketed depth; n: ratio of rock-socketed depth, $n = h/D$.

(a) (b)

Figure 3: Properties of the materials. (a) General prefabricated piles. (b) Steel tube prefabricated piles.

Table 6: Material properties of the concrete core and steel tube.

Steel tube	Concrete	Reinforced bar	Steel tube (mm)
$D = 100$ mm	M30	$D = 6$ mm	$E_c = 16$ MPa
$t = 1$ mm	—	—	$f_y = 300$ KPa
$E_s = 200$ GPa	C : S : $W = 1 : 1.76 : 0.32$	—	—

jack is fixed to the reaction beam, and the device diagram is shown in Figure 4. During step-by-step loading, to keep each load the same, the load is calculated according to 10% of the estimated carrying capacity. The first stage load is 2 times the grading load; the unloading is reduced by a consistent 20% of the carrying capacity. The requirements are that the transmission load is uniform, continuous, and stable and that the time of loading is at least 1 minute.

3. Test Results and Discussion

3.1. Columns without Foundation

3.1.1. Failure Modes. The typical failure modes of the specimens in this test are as follows. The failure modes of the plain concrete specimen (PL-2) and the reinforced concrete specimen (RN-2) are shown in Figures 5(a) and 5(b). The main failure mode is the fracture of the top concrete, and the crushing range is about one quarter of the length of the pile.

The typical failure mode of the unreinforced CFST specimens (NS-A-2 and NS-B-2) is shown in Figure 5(c), which is mainly represented by the local buckling of the specimen after concrete crushing.

The reinforced CFST piles exhibit two different failure modes. The specimens with the thickness of 1.6 mm of steel casing (RS-B-1 and RS-B-2) locally exhibit buckling deformation during loading, the local deformation is gradually increased with the loading, and the specimen is bent and deformed until the bearing capacity is finally lost, as shown in Figure 6(a). The specimens with the thickness of 1.2 mm (RS-A-1 and RS-A-2) showed the same deformation characteristics as the specimen RS-B-1 in the early stage of loading, but when the load reaches 850 kN, the weld of the steel casing suddenly opened. The specimen is destroyed instantaneously, as shown in Figure 6(b). In summary, two different types of damage may occur in reinforced CFST when axially compressed:

(1) When the weld strength of the steel casing is greater than the axial load limit of the composite member, the failure mode is the bending failure caused by the local buckling deformation, which is a ductile failure feature

(2) When the weld strength of the steel casing is less than the axial load limit of the composite member, the failure mode is the open splitting of the steel casing weld under the expansion stress of the concrete, which is a brittle failure feature

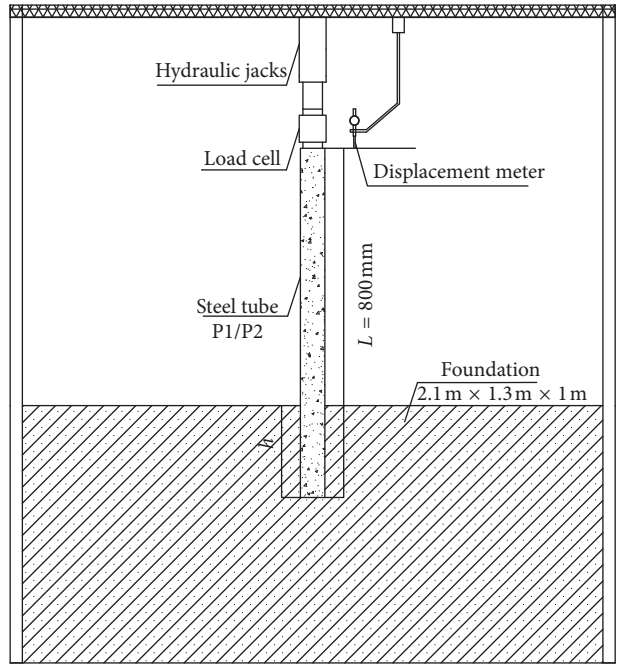

Figure 4: Test setup (h means rock-socketed depth; P1: steel tube is 1 mm; P2: steel tube is 0 mm).

3.1.2. Load-Displacement Curve

(1) Reinforced and Unreinforced CFST Members. The load-vertical displacement curves of reinforced CFST specimens with steel casing thickness of 1.2 mm (RS-A-2) and 1.6 mm (RS-B-2) are shown in Figure 7. It can be seen from the test results that when the thickness of the steel casing increases to 1.6 mm, the displacement of the top of the specimen with the load is the same as that of the thickness of 1.2 mm, and both exhibit obvious plastic failure properties, the proportional limit of two thicknesses is relatively close, which is approximately 600 kN. Before the load reaches 600 kN, the load-displacement curves of the two test pieces are basically coincident. When the load exceeds 600 kN, that is, after entering the plastic zone, the absolute value of the displacement increment under the same load increment is smaller than the case where the thickness of the steel casing is 1.2 mm under the same condition. It indicates that the restraining effect of the steel casing on the core concrete is mainly reflected in the plastic zone of the component, while the effect on the elastic zone is small. The maximum displacement that can be achieved with a thickness of 1.6 mm is 13.8 mm, which is greatly improved compared to the thickness of the steel casing of 1.2 mm. Therefore, the thickness of the steel casing has a great influence on the ductility of the reinforcing member and the improvement of its bearing capacity.

The load-vertical displacement curves of CFST specimens with steel tube thickness is 1.2 mm (RS-A-2 and NS-A-2) and t steel tube thickness is 1.6 mm (RS-B-2 and NS-B-2) composite members are shown in Figures 8 and 9.

(a) (b)

(c)

Figure 5: Failure modes. (a) Plain concrete pile. (b) Reinforced concrete pile. (c) Unreinforced CFST pile.

It can be obtained from the test results that the proportional limit of the load-vertical displacement curve of reinforced CFST piles is slightly higher than unreinforced ones and the proportional limit of the specimen RS-A-2 and RS-B-2 is about 600 kN, greater than 500 kN of test NS-A-2 and NS-B-2. At the same time, the ultimate deformation capacity of reinforced CFST composite members is better than that of unreinforced CFST specimens. It can be seen that in the elastic stress stage, the presence of the stressed steel bars delays the generation of concrete cracks, thereby increasing the proportional limit of the test. In the plastic stage, the stressed steel bars play a further restraining role on the core concrete, which inhibits the formation and expansion of the crack and improves the ductility and ultimate deformation ability of the test.

(2) Encased and Nonencased Members. The load-vertical displacement curves of plain concrete specimen (PL-2) and reinforced concrete specimen (RN-2) and reinforced CFST composite members (RS-A-2 and RS-B-2) are shown in Figure 10. It can be seen from the test results that the steel tube has a great influence on the bearing capacity and deformation capacity of the test. For the plain concrete specimen (PL-2), the ultimate bearing capacity and ultimate deformation are small, and the maximum displacement is 2.87 mm, showing the characteristics of brittle failure. For the

(a) (b)

Figure 6: Failure modes of reinforced CFST pile. (a) Buckling deformation. (b) Splitting of the steel casing weld.

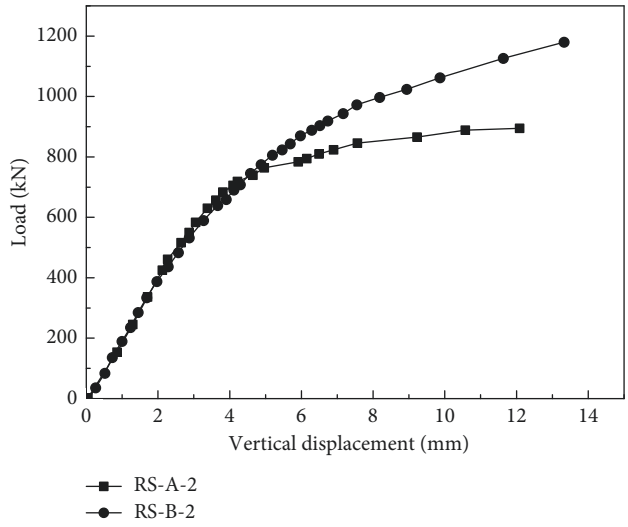

Figure 7: Vertical displacement-load curves of two thickness steel tube-reinforced CFST piles.

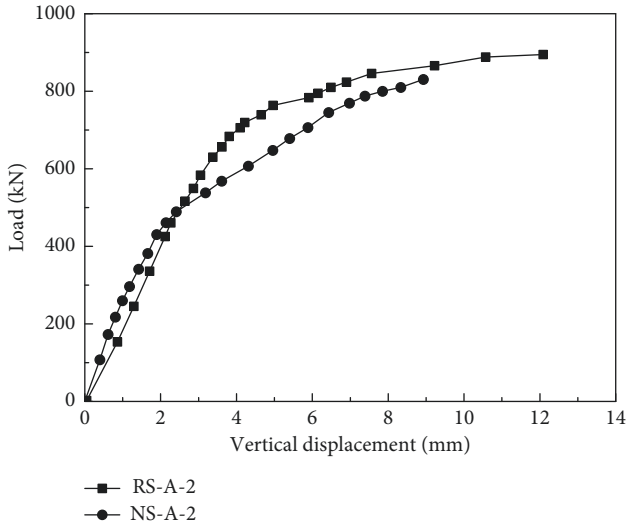

Figure 8: Comparison of reinforced and unreinforced CFST piles with thickness is 1.2 mm.

reinforced concrete specimen (RN-2), the load-displacement curve shows a certain ductility characteristic, but the ultimate bearing capacity and ultimate deformation of the specimen are significantly smaller than the reinforced CFST composite member.

3.1.3. Strain Development. In this paper, the strain law of the steel casing and concrete core under the condition of an axial compression load is described for the specimens with a steel tube thickness of 1.2 mm (specimen RS-A-2) and 1.6 mm (specimen RS-B-2). During the test, the vertical strain and hoop strain on the side of the steel casing were monitored and the development rule of the compressive strain inside the core concrete was monitored. Among them, four strain gauges are arranged on the side of the steel casing at the top and middle and top of the test specimen in the circumferential direction, and the vertical strain and lateral strain of the steel casing at this position are measured, respectively. In the data processing, the strain values of four measuring points in the same plane are averaged to obtain the average strain of the steel casing at the plane. The load-strain curve and average stress-strain curve of the test piece are given below. Among them, the average stress is obtained by dividing the axial load on the specimen by the cross-sectional area.

The developments of the longitudinal strain, circumferential strain, and compression behavior of the steel tube are shown in Figures 11–16. Figures 11–13 are laws of strain

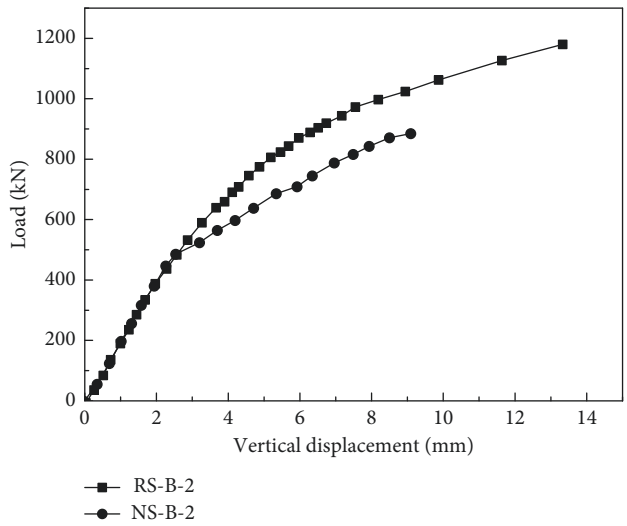

Figure 9: Comparison of reinforced and unreinforced CFST piles with thickness is 1.6 mm.

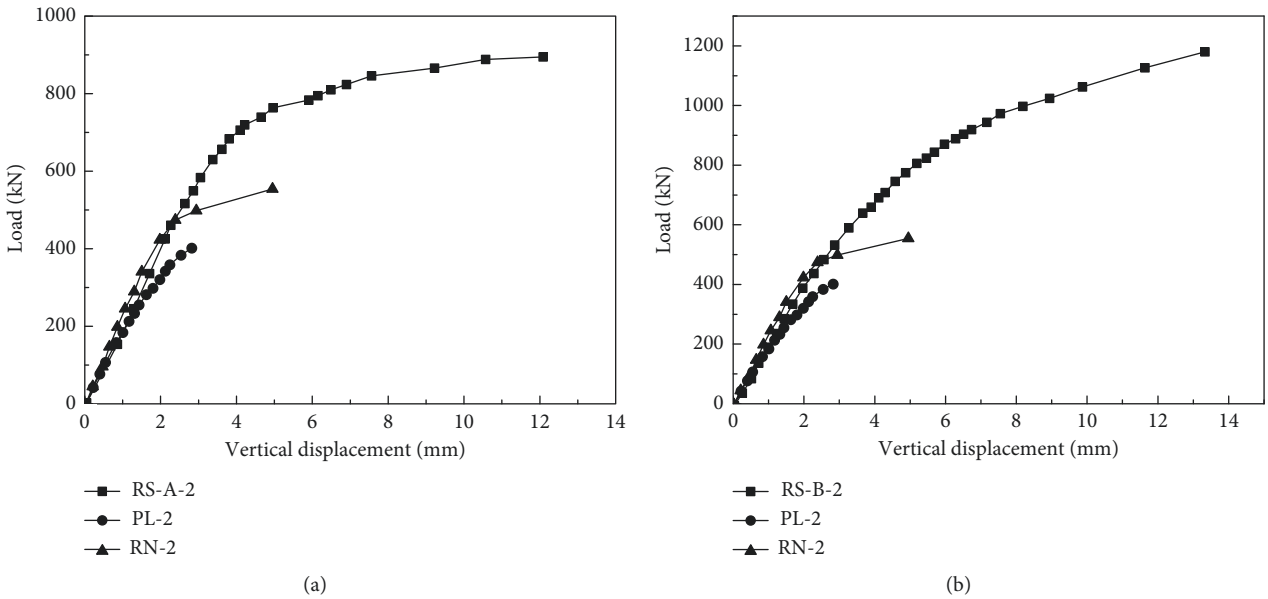

Figure 10: Comparison of plain concrete, reinforced concrete, and reinforced CFST piles.

development of specimen RS-A-2, and Figures 14–16 are laws of strain development of specimen RS-B-2.

From the above test results, it can be seen that for the steel casing-reinforced concrete composite member, the strain value in the middle of the specimen is slightly larger than the top and bottom strain values. The strain development of steel casings at each measuring point shows elastic-plastic characteristics with the increase of load. Before the axial load value is less than 0.45 times, the ultimate load of the model pile foundation, the load, and strain show a linear relationship, while the load reaches 0.45 times the ultimate load carrying capacity. After the capacity, under the same load increment, the strain increment gradually increases, showing a nonlinear characteristic. From the whole load-strain curves of the reinforced CFST specimens, it exhibited the characteristics of ductile failure.

In summary, the use of a steel tube plays a very important role in improving the compressive deformation and mechanical properties of the components. For a joint steel tube-reinforced concrete structure, the bearing capacity and the ductility of the components are greatly improved compared to the specimens with no steel, which is due to the existence of the internal structure of the composite structure, effectively enhancing the constraints between the concrete particles to limit the development of microcracks and the effective stress.

3.2. Columns with Foundation. It can be seen from Figure 17 that the variation in the results of the different model columns under the load at the pile top is consistent, and it can be considered that the influence of a rockless cylinder on the

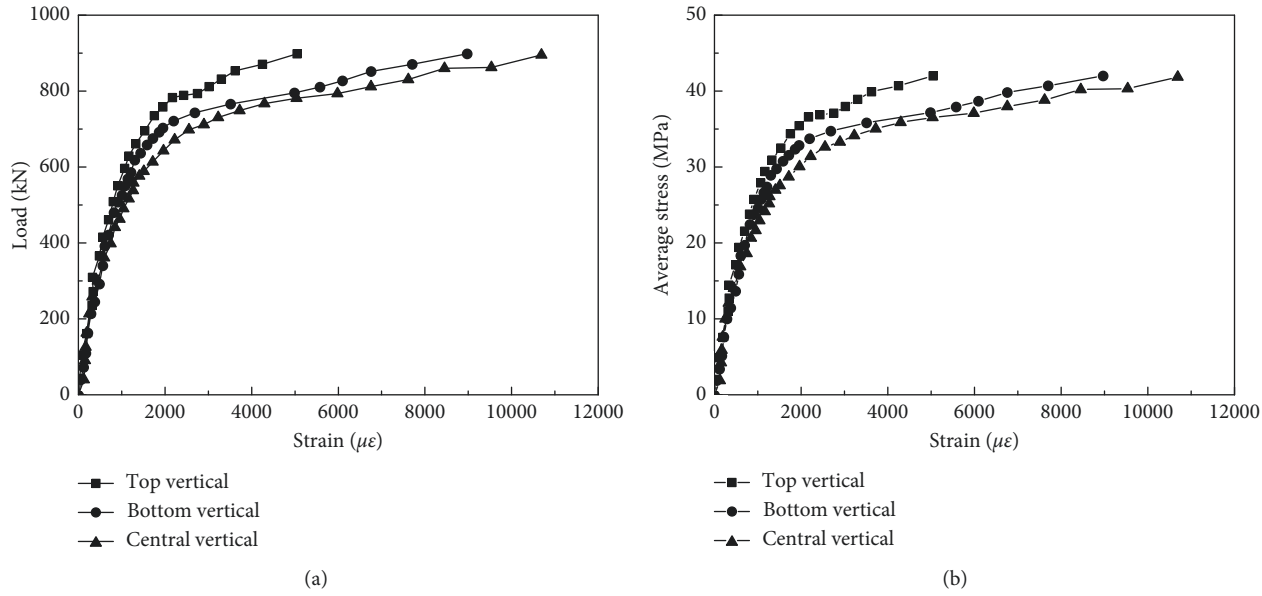

Figure 11: Vertical strain development laws of specimen RS-A-2 with steel casing. (a) Relationship of vertical strain development with load. (b) Relationship of vertical strain development with average stress.

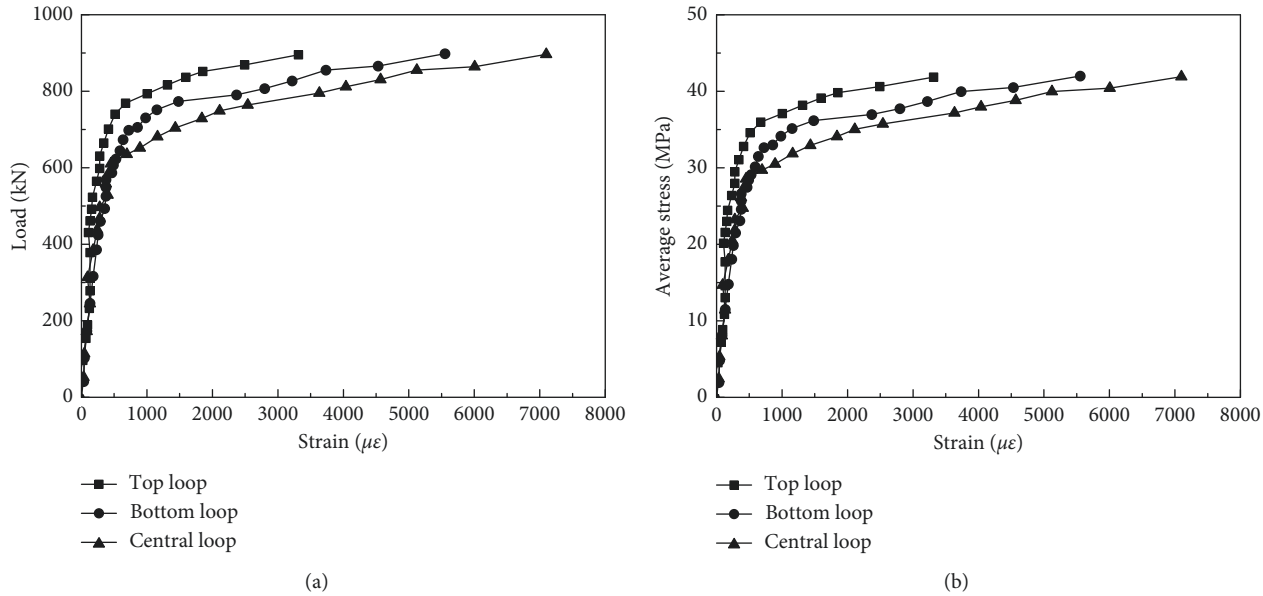

Figure 12: Loop strain development of specimen RS-A-2 with steel casing. (a) Relationship of loop strain development with load. (b) Relationship of loop strain development with average stress.

settlement of a rock-socketed column is also consistent. It can be seen from Figure 17 that the displacements of Z1P1 and Z1P2 are basically the same from the load values of zero to 9 kN, the load-vertical displacement curve is approximately a straight line, and the two piles are in the elastic stage. After the load exceeds 9 kN, the displacement rate of the Z1P1 pile exceeds that of the Z1P2 pile and the settlement of the pile top increases. The load-vertical displacement curves of the two piles change slowly, and the process of steep drop is not obvious. Figure 17 shows several settlings that may be due to the inhomogeneity of the model foundation. According to the above analysis, it can be seen that the vertical bearing capacities of CFST rock-socketed piles are weaker than those rock-socketed piles without a steel tube; the difference is mainly because the rock-socketed pile without a steel tube has a concrete-rock interface with a coefficient of friction greater than that of the CFST rock-socketed pile with a steel-rock interface.

As seen from Figure 18, the greater the rock-socketed depth, the greater the load-bearing capacity of the rock-socketed piles. In addition, when the depth of the pile in the rock-socketed increased from 3D to 5D, the vertical ultimate

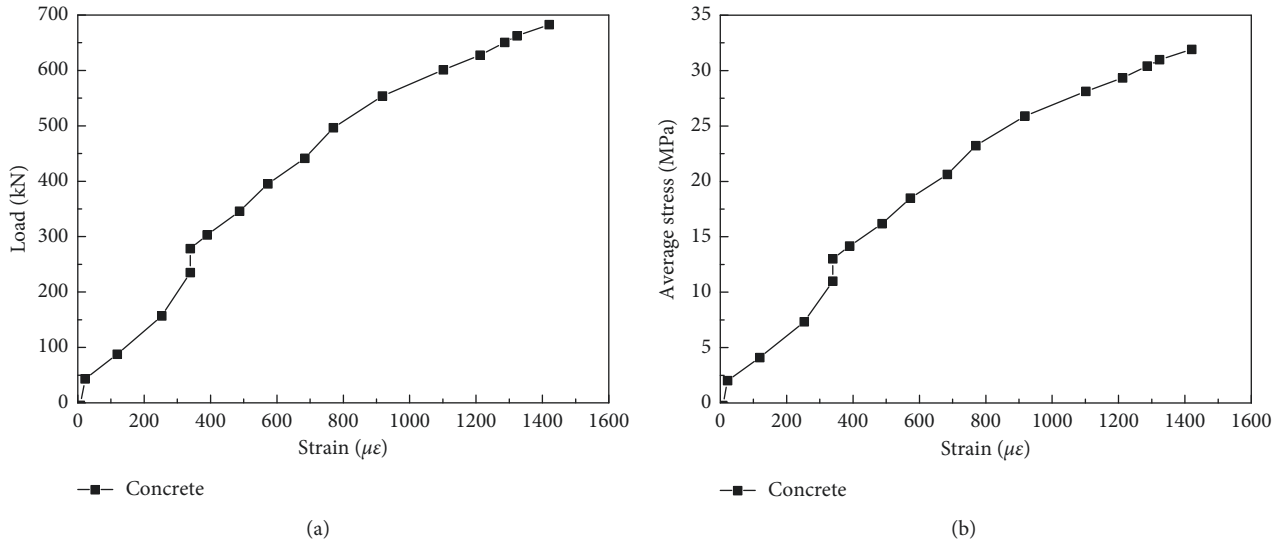

Figure 13: Axial compressive strain development of core concrete of specimen RS-A-2. (a) Relationship of vertical strain development with load. (b) Relationship of vertical strain development with average stress.

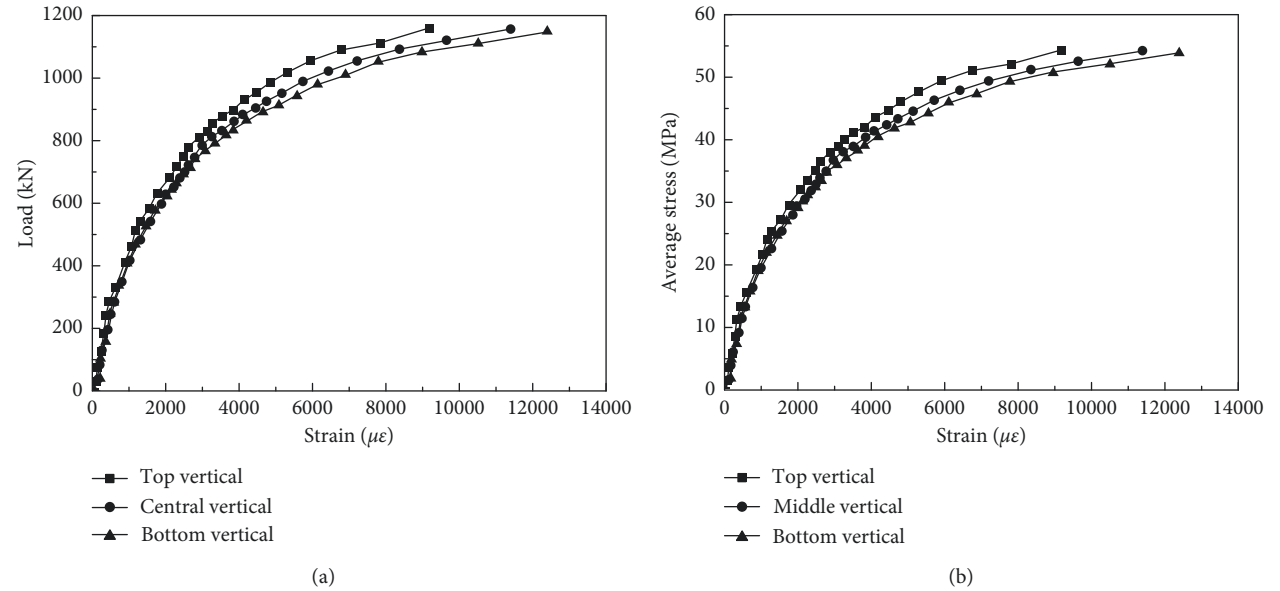

Figure 14: Vertical strain development laws of specimen RS-B-2 with steel casing. (a) Relationship of loop strain development with load. (b) Relationship of loop strain development with average stress.

bearing capacity increased by approximately 40%. The main reason for this effect is that with the increase in the rock-socketed depth, the contact area will increase, and although the side friction coefficient does not change, the total friction of the pile will significantly increase; therefore, the vertical bearing capacity of the pile is significantly improved. It is found that the vertical ultimate bearing capacity of rock-socketed piles without a steel tube (steel-free cylinder) is approximately 10% higher than that of the steel-retaining tube when the depth of rock-embedment is the same. The main reason for this phenomenon is that the outer wall of the pile is very smooth; since its roughness is much smaller than the concrete, the corresponding side friction is lower, and the ultimate bearing capacity of the pile is equal to the pile side friction and pile end resistance, decreasing the ultimate bearing capacity of the pile.

4. Analysis of the Ultimate Load

According to EC4 [22], the axial load capacity ($N_{\mathrm{pl,Rd}}$) of a CFST column can be determined by summing the yield load of both the steel section and concrete core. For concrete-fined tubes of circular cross section, account may be taken of increase in strength of concrete caused by confinement provided that the relative slenderness $\overline{\lambda}$ does not exceed 0, 5, and $e/d < 0$, 1, where e is the eccentricity of

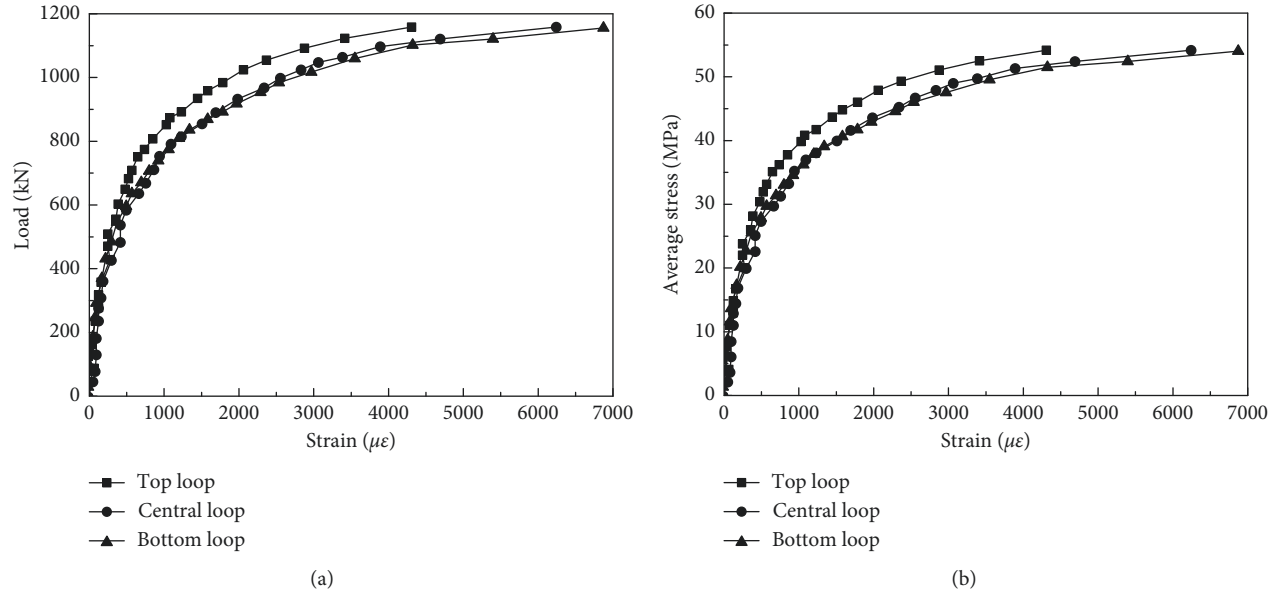

Figure 15: Loop strain development of specimen RS-B-2 with steel casing. (a) Relationship of strain development with load. (b) Relationship of strain development with average stress.

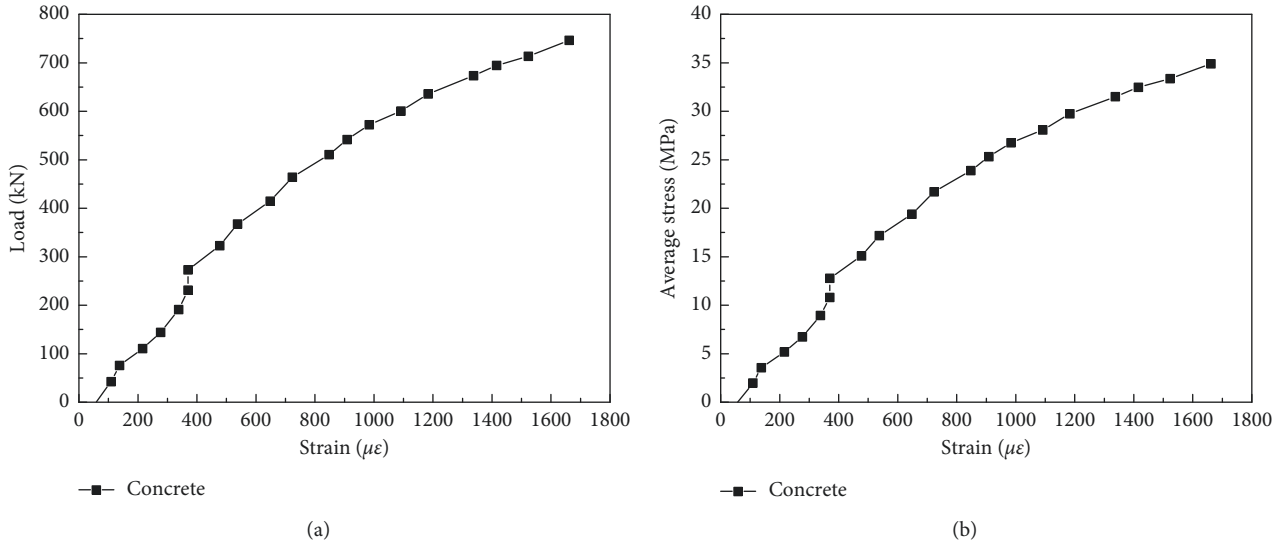

Figure 16: Axial compressive strain development of core concrete of specimen RS-B-2.

loading given by M_{Ed}/N_{Ed} and d is the external diameter of the column. The plastic resistance to compression may then be calculated from the following expression in equations (2)–(5). The application of EC4 [22] is restricted to composite columns with steel yield stress and concrete cylinder strength of less than 355 and 50 MPa, respectively. The following presents the formulations of the AISC [21], EC4 [22], NBR 8800 [23, 24], and GB50396-2014 [25] standard codes to determine the resistance capacity of axially loaded CFST columns. And r_s is the radius of gyration of the steel hollow section, l_e is the length of the column, E_c is the modulus of elasticity of the concrete, and E_s is the modulus of elasticity of the steel. The formulations presented were used to calculate the compressive strength of the axially loaded CFST columns investigated in the present study. In addition, the boundary conditions of the testing approach are upper if the pile is loading and lower if the pile is fixed.

In GB50396-2014 [25], θ means the hoop coefficient of concrete-filled steel tubular members $\theta = \alpha_{sc} f / f_c$, α_{sc} represents the steel content of concrete-filled steel tubular members, in the design of compressive strength of concrete-filled steel tube piles, B and C are the influence factors of the cross-sectional shape on the hoop effect, and about circular cross section, $B = 0.176 * f/213 + 0.974$, $C = -0.104 f_c/14.4 + 0.031$. In AISC [21], the axial compression member is considered to be the overall stability of the member, the

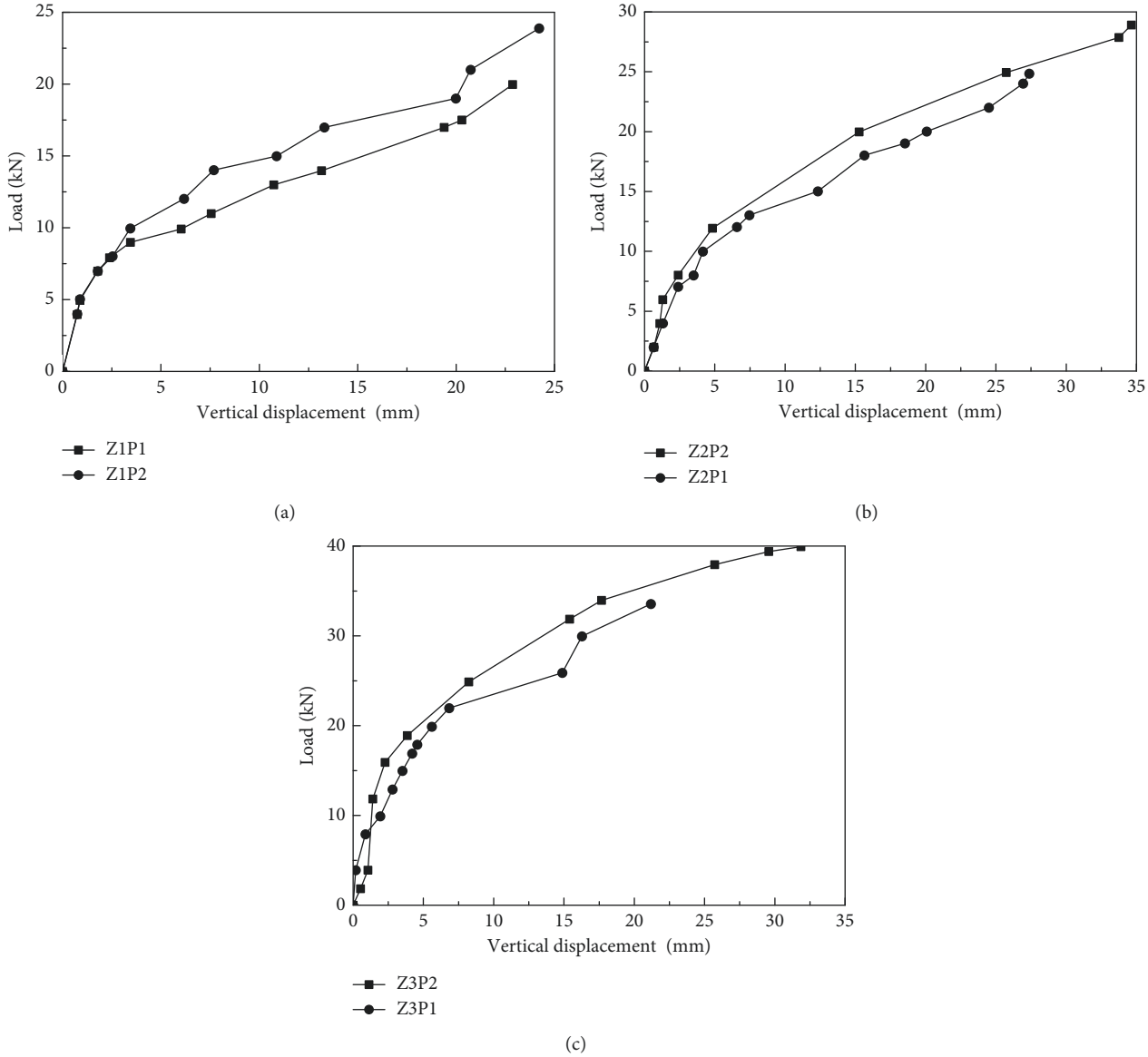

FIGURE 17: Relationship of vertical displacement and load of three depths of rock-socketed columns. (a) Rock-socketed depth is 300 mm (P1: steel tube is 1 mm; P2: steel tube is 0 mm). (b) Rock-socketed depth is 400 mm. (c) Rock-socketed depth is 500 mm.

strength of the concrete is converted into the steel, the nominal compressive strength f_{cr} of the steel is obtained, and the bearing capacity of the concrete-filled steel tubular member is calculated from f_{cr}, f_{ys} is the yield limit of steel, f_{ck} means the compressive strength of concrete cylinder, A_s is the cross-sectional area of steel pipe, A_c is the cross-sectional area of concrete, and λ_c is the ratio of slenderness to slenderness. In Eurocode 4 (EC4) [22], the relative slenderness $\overline{\lambda}$ for the plane of bending being considered is given by $\overline{\lambda} = \sqrt{N_{PL,Rk}/N_{cr}}$, where $N_{pl,Rk}$ is the characteristic value of the plastic resistance to compression if, instead of the design strengths, the characteristic values are used and N_{cr} is the elastic critical normal force for the relevant buckling mode, calculated with the effective flexural stiffness $(EI)_{cff}$.

However, it should be stated that the maximum allowable value of diameter-thickness ratio (D/t) specified in AISC [21] is $0.31 * E/f_y$; the ratio of diameter-thickness of circular-section concrete-filled steel tubular members specified in Chinese specification [28] should be limited to the following range: $20\sqrt{235/f_y} \le D/t \le 85\sqrt{235/f_y}$; and Eurocode 4 (EC4) [22] explicit limits the allowed D/t values in the European context to $90 * 235/f_y$. The diameter-thickness ratio of the specimens studied in this paper is very large, exceeding the allowable range of the specifications. The paper attempts to estimate these specimens with large diameter-thickness ratio by using the above codes. And the ultimate strength calculation results of relevant specifications are shown in Table 7. Apparently, it can be found that value of the ultimate load is generally much greater than the theoretical calculation results.

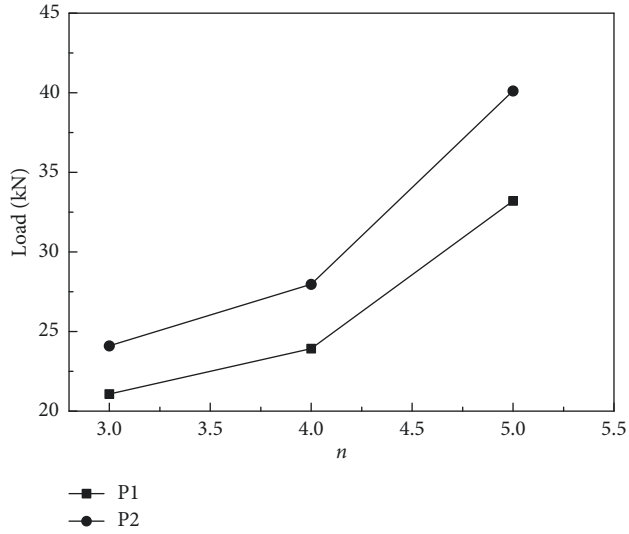

Figure 18: Relationship between n and load (n: ratio of rock-socketed depth, $n = h/D$).

Table 7: The ultimate strength calculation results of relevant specifications.

Specimens	Ultimate load (kN)	NBR 8800 and EC4 (kN)	AISC (kN)	GB50396-2014 (kN)
PL-2	406	412	419	429
NS-A-2	830	493	479	560
NS-B-2	885	566	535	603
RN-2	560	430	416	465
RS-A-2	895	493	479	596
RS-B-2	1190	566	535	639
PL-1	480	513	519	530
NS-A-1	800	428	409	478
RS-A-1	895	428	409	478
RS-B-1	1125	452	474	498

AISC [21] method:

$$
\begin{aligned}
E_{\mathrm{m}} &= E_{\mathrm{s}} + 0.4E_{\mathrm{c}}\frac{A_{\mathrm{c}}}{A_{\mathrm{s}}},\\
f_{\mathrm{my}} &= f_{\mathrm{ys}} + 0.85f_{\mathrm{ck}}\frac{A_{\mathrm{c}}}{A_{\mathrm{s}}},\\
f_{\mathrm{cr}} &= \left(0.658^{\lambda_{\mathrm{c}}^2}\right)f_{\mathrm{my}} \quad \text{if } \lambda_{\mathrm{c}} \le 1.5,\\
f_{\mathrm{cr}} &= \frac{0.877}{\lambda_{\mathrm{c}}^2}f_{\mathrm{my}} \quad \text{if } \lambda_{\mathrm{c}} \le 1.5,\\
\lambda_{\mathrm{c}} &= \frac{l_{\mathrm{c}}}{r_{\mathrm{c}}\pi}\left(\frac{f_{\mathrm{my}}}{E_{\mathrm{m}}}\right)^{0.5},\\
N_{\mathrm{pl.Rd}} &= 0.85A_{\mathrm{s}}f_{\mathrm{cr}}.
\end{aligned}
\tag{1}
$$

EC4 and NBR 8800 [23, 24] methods:

$$
N_{\mathrm{pl.Rd}} = \eta_2 A_s f_{\mathrm{y}} + A_{\mathrm{c}} f_{\mathrm{ck}}\left(1 + \eta_1\frac{t f_{\mathrm{y}}}{D f_{\mathrm{ck}}}\right), \tag{2}
$$

$$
\begin{aligned}
\eta_1 &= \eta_{10},\\
\eta_2 &= \eta_{20},
\end{aligned}
\tag{3}
$$

$$
\eta_{10} = 4.9 - 18.5 \times \overline{\lambda} + 17(\overline{\lambda})^2 \ge 0, \tag{4}
$$

$$
\eta_{20} = 0.25(3 + 2\overline{\lambda}) \le 1.0. \tag{5}
$$

GB50396-2014 [25] method:

$$
\begin{aligned}
N_0 &= A_{\mathrm{sc}}f_{\mathrm{sc}},\\
f_{\mathrm{sc}} &= \left(1.212 + B\theta + C\theta^2\right)f_{\mathrm{c}},\\
\alpha_{\mathrm{sc}} &= \frac{A_{\mathrm{s}}}{A_{\mathrm{c}}},\\
\theta &= \alpha_{\mathrm{sc}}\frac{f}{f_{\mathrm{c}}}.
\end{aligned}
\tag{6}
$$

5. Conclusion

The present study is an attempt to study the behavior of concrete-filled steel tube columns subjected to axial compression. Based on the results of this study, the following conclusions can be drawn within the scope of these tests:

(1) The reinforced CFST piles exhibit two different failure modes. When the weld strength of the steel casing is greater than the axial load limit of the composite member, the failure mode is the bending failure caused by the local buckling deformation, which is a ductile failure feature. When the weld strength of the steel casing is less than the axial load limit of the composite member, the failure mode is the open splitting of the steel casing weld under the expansion stress of the concrete, which is a brittle failure feature.

(2) The bearing capacity of rock-socketed CFST columns is lower than that of rock-socketed columns without a steel tube under the same conditions of a vertical load. The depth of the rock inlay is clearly affecting by the bearing capacity of the two rock-socketed columns, and the greater the rock-socketed depth, the greater the bearing capacity of the rock-socketed piles. In addition, the overall sliding of the steel tube and the core concrete of pile is small, and the steel tube-concrete interface is basically in a bonding state under the vertical load.

(3) A comparison of failure loads between the tests and the design codes was presented. The results show that the provisions in EC4 [22], NBR 8800 [23, 24], AISC [21], and GB50396-2014 [25]conservatively estimate the ultimate capacities of the specimens, and it can be found that value of the ultimate load is generally much greater than the theoretical calculation results. Since the diameter-thickness ratio of the specimens studied in this paper is very large, exceeding the allowable range of the specifications, the test results provide a reference for design and performance of the new structure with large diameter-thickness ratio.

Data Availability

The figures and tables data used to support the findings of this study are included within the article.

Conflicts of Interest

The authors declare that there are no conflicts of interest regarding the publication of this paper.

Acknowledgments

This study was financially supported by the National Natural Science Foundation of China (nos. 2011550031 and 51709026) and the Western Project of China (nos. 2011660041 and 2011560076).

References

[1] S. Jegadesh and S. Jayalekshmi, "Load-bearing capacity of axially loaded circular concrete-filled steel tubular columns," *Proceedings of the Institution of Civil Engineers: Structures and Buildings*, vol. 169, no. 7, pp. 508–523, 2016.

[2] N. E. Shanmugam and B. Lakshmi, "State of the art report on steel–concrete composite columns," *Journal of Constructional Research*, vol. 57, no. 10, pp. 1041–1080, 2001.

[3] S. De Nardin, "*Theoretical-experimental study high strength concrete-filled steel tubes*," M.S. thesis, EESC-USP, Sao Carlos-SP, 1999, in Portuguese.

[4] K. Cederwall, B. Engstrom, and M. Grauers, "High-strength concrete used in composite columns," in *Proceedings of High-Strength Concrete–2nd International Symposium*, pp. 195–214, Detroit, MI, USA, 1990.

[5] L. Han, W. Li, and R. Bjorhovde, "Developments and advanced applications of concrete-filled steel tubular (CFST) structures: members," *Journal of Constructional Steel Research*, vol. 100, pp. 211–228, 2014.

[6] L. Han, H. Shan-Hu, and F. Liao, "Performance and calculations of concrete filled steel tubes (CFST) under axial tension," *Journal of Constructional Steel Research*, vol. 67, no. 11, pp. 1699–1709, 2011.

[7] M. A. Bradford, "Design strength of slender concrete filled rectangular steel tubes," *ACI Structural Journal*, vol. 93, no. 2, pp. 229–235, 1996.

[8] M. D. O'Shea and R. Q. Bridge, "Design of thin-walled concrete filled steel tubes," *Journal of Structural Engineering*, vol. 126, no. 11, pp. 1295–1303, 2000.

[9] B. Uy, "Local and postlocal buckling of fabricated steel and composite cross sections," *Journal of Structural Engineering*, vol. 127, no. 6, pp. 666–677, 2001.

[10] K. K. Choi and Y. Xiao, "Analytical studies of concrete-filled circular steel tubes under axial compression," *Journal of Structural Engineering*, vol. 136, no. 5, pp. 565–573, 2010.

[11] Z. Ou, B. Chen, K. H. Hsieh, M. W. Halling, and P. J. Barr, "Experimental and analytical investigation of concrete filled steel tubular columns," *Journal of Structural Engineering*, vol. 137, no. 6, pp. 635–645, 2011.

[12] T. Perea, R. T. Leon, J. F. Hajjar, and M. D. Denavit, "Full-scale tests of slender concrete-filled tubes: axial behavior," *Journal of Structural Engineering*, vol. 139, no. 7, pp. 1249–1262, 2013.

[13] L. H. Han, "Flexural behavior of concrete-filled steel tubes," *Journal of Constructional Steel Research*, vol. 60, no. 2, pp. 313–337, 2004.

[14] L. H. Han, "Further study on the flexural behavior of concrete-filled steel tubes," *Journal of Constructional Steel Research*, vol. 62, no. 6, pp. 554–565, 2006.

[15] H. Lu, L. H. Han, and X. L. Zhao, "Analytical behavior of circular concrete-filled thin-walled steel tubes subjected to bending," *Thin-Walled Structures*, vol. 47, no. 3, pp. 346–358, 2009.

[16] C. W. Roeder, D. E. Lehman, and E. Bishop, "Strength and stiffness of circular concrete-filled tubes," *Journal of Structural Engineering*, vol. 136, no. 12, pp. 1545–1553, 2010.

[17] J. Moon, C. W. Roeder, D. E. Lehman, and H. Lee, "Analytical modeling of bending of circular concrete-filled steel tubes," *Engineering Structures*, vol. 42, pp. 349–361, 2012.

[18] L. H. Han, G. H. Yao, and Z. Tao, "Performance of concrete-filled thin-walled steel tubes under pure torsion," *Thin-Walled Structures*, vol. 45, no. 1, pp. 24–36, 2007.

[19] J. Nie, Y. Wang, and J. Fan, "Experimental study on seismic behavior of concrete filled steel tube columns under pure torsion and compression–torsion cyclic load," *Journal of Constructional Steel Research*, vol. 79, no. 12, pp. 115–126, 2013.

[20] Y. Wang, J. Nie, and J. Fan, "Theoretical model and investigation of concrete filled steel tube columns under axial

force–torsion combined action," *Thin-Walled Structures*, vol. 69, no. 1, pp. 1–9, 2013.

[21] American Institute of Steel Construction, *AISC–LRFD: Metric Load and Resistance Factor Design Specification for Structural Steel Buildings*, AISC, Chicago, IL, USA, 1994.

[22] Europe en Comite de Normalisation, *ENV 1994–1–1: Eurocode 4—Design of Composite Steel and Concrete Structures, Part 1.1: General Rules and Rules for Buildings*, CEN, Brussels, Belgium, 1994.

[23] Brazilian Society of Standard Codes, *NBR 8800: Design and Constructional Details of Steel Structures of Buildings*, Brazilian Society of Standard Codes, Rio de Janeiro, Brazil, 1986.

[24] Brazilian Society of Standard Codes, *NBR 8800 Brazilian Standard Code Review: Design and Constructional Details of Steel and Composite Structures of Buildings*, BSSC, Belo Horizonte, Brazil, 2003.

[25] National Standards of the People's Republic of China, *GB 50936, Technical Code for Concrete Filled Steel Tubular Structures*, National Standards of the People's Republic of China, Beijing, China, 2014, in Chinese.

[26] Q. Liu, D. Wang, R. Huang et al., "Study on failure mode of inland river large water level dock under ship impact," *Port Engineering Technology*, vol. 47, no. 4, 2010, in Chinese.

[27] J. Xu, "Structural design of overhead vertical wharf for inland river large water level," *Water Transport Engineering*, vol. 2006, pp. 62–67, 2006, in Chinese.

[28] China Association for Engineering Construction Standardization, *CECS 28:90: Specification for Design and Construction of Concrete-Filled Steel Tubular Structures*, China Association for Engineering Construction Standardization, Beijing, China, 2012, in Chinese.